Nanoscale

PAPER

View Article Online
View Journal | View Issue

Cite this: *Nanoscale*, 2023, **15**, 532

Complex ligand adsorption on 3D atomic surfaces of synthesized nanoparticles investigated by machine-learning accelerated *ab initio* calculation†

Dohun Kang, ‡[a,b] Sungin Kim, ‡[a,c] Junyoung Heo, [a,c] Dongjun Kim,[a] Hyeonhu Bae,[d] Sungsu Kang,[a,c] Sangdeok Shim,*[e] Hoonkyung Lee*[d] and Jungwon Park *[a,c,f,g]

Nanoparticle surfaces are passivated by surface-bound ligands, and their adsorption on synthesized nanoparticles is complicated because of the intricate and low-symmetry surface structures. Thus, it is challenging to precisely investigate ligand adsorption on synthesized nanoparticles. Here, we applied machine-learning-accelerated *ab initio* calculation to experimentally resolved 3D atomic structures of Pt nanoparticles to analyze the complex adsorption behavior of polyvinylpyrrolidone (PVP) ligands on synthesized nanoparticles. Different angular configurations of large-sized ligands are thoroughly investigated to understand the adsorption behavior on various surface-exposed atoms with intrinsic low-symmetry. It is revealed that the ligand binding energy (E_{ads}) of the large-sized ligand shows a weak positive relationship with the generalized coordination number ($\overline{CN}$). This is because the strong positive relationship of short-range direct bonding (E_{bind}) is attenuated by the negative relationship of long-range van der Waals interaction (E_{vdW}). In addition, it is demonstrated that the PVP ligands prefer to adsorb where the long-range vdW interaction with the surrounding surface structure is maximized. Our results highlight the significant contribution of vdW interactions and the importance of the local geometry of surface atoms to the adsorption behavior of large-sized ligands on synthesized nanoparticle surfaces.

Received 26th September 2022,
Accepted 5th December 2022

DOI: 10.1039/d2nr05294f

rsc.li/nanoscale

Introduction

Surface-bound ligands determine the structures of colloidal nanoparticles by regulating the surface energy and growth pathway in the synthesis. In addition, the physicochemical properties of the synthesized nanoparticles are sensitive to the binding type and surface distribution of the ligands.[1–3] There are different types of ligands used in the synthesis of nanoparticles, including polymers, organic molecules, inorganic complexes, and metal ions. Among them, polymers such as polyvinylpyrrolidone (PVP) are widely used to direct the structures of metal nanoparticles, exploiting their preferential adsorption on different crystallographic surfaces.[4–6]

Several experimental methods including infrared spectroscopy, nuclear magnetic resonance spectroscopy, and X-ray photoelectron spectroscopy are extensively used to investigate the ligand-binding chemistry on the nanoparticle surface.[7–10] However, they are based on spectroscopic information from the nanoparticle ensemble and have limitations in investigating ligand interactions at the single particle level. Theoretical calculations based on quantum mechanics are employed to understand the adsorption chemistry of ligands with high accuracy,[10–14] but are not yet readily applicable to synthesized nanoparticles with complex surface structures and large-sized ligand systems. The complex surfaces of synthesized nanoparticles having low-symmetry surface atoms, edges, and corners require extremely large computational

[a]*School of Chemical and Biological Engineering, Institute of Chemical Processes, Seoul National University, Seoul 08826, Republic of Korea. E-mail: jungwonpark@snu.ac.kr*
[b]*Department of Materials Science and Engineering, Northwestern University, Evanston, Illinois 60208, USA*
[c]*Center for Nanoparticle Research, Institute for Basic Science (IBS), Seoul 08826, Republic of Korea*
[d]*Department of Physics, Konkuk University, Seoul 05029, Republic of Korea. E-mail: hkiee3@konkuk.ac.kr*
[e]*Department of Chemistry, Sunchon National University, Suncheon 57922, Republic of Korea. E-mail: san90@scnu.ac.kr*
[f]*Institute of Engineering Research, College of Engineering, Seoul National University, 1 Gwanak-ro, Gwanak-gu, Seoul 151-742, Republic of Korea*
[g]*Advanced Institutes of Convergence Technology, Seoul National University, 145, Gwanggyo-ro, Yeongtong-gu, Suwon-si, Gyeonggi-do, 16229, Republic of Korea*
†Electronic supplementary information (ESI) available. See DOI: https://doi.org/10.1039/d2nr05294f
‡These authors contributed equally to this work.

resources. In addition, large-sized ligand systems have configurational degrees of freedom along the different adsorption directions and complex binding modes including van der Waals interaction.

Recently, several sampling methods based on machine learning have been proposed for fast and precise computation of adsorption energy on the surface of nanoparticles. They are successful with small molecular adsorbates such as H, CO and HCHO.[15–17] The accuracy and efficiency exhibited by artificial neural network (ANN) prediction for small molecules encourage us to investigate the complex surface interactions of polymer ligands used in the synthesis of nanoparticles by using the ANN. Here, we studied ligand binding characteristics in a synthesized nanoparticle–ligand system – Pt nanoparticles passivated by PVP ligands – using machine-learning-accelerated *ab initio* calculation. We applied an ANN to the realistic 3D atomic structure of the synthesized nanoparticles that we directly analyzed from their colloidal phase with a precision of 19 pm. This enabled the efficient scanning of the binding interactions of a large-sized ligand on intrinsically disordered surfaces of colloidal nanoparticles without extended computation for structural relaxation. As a result, the energy, modes, and orientations of ligand binding were thoroughly investigated for 1334 surface atomic sites of 6 Pt nanoparticles with high precision. The results reveal that the short-range direct bonding prefers less-coordinated adsorption sites, while the long-range van der Waals interaction of PVP becomes stronger with more neighboring surface atoms, contributing to the overall binding affinity of PVP on the surfaces of the synthesized Pt nanoparticles. In addition, it is found that the contribution from van der Waals interaction is important in the passivation of the nanoparticle surfaces by long ligands such as PVP polymers.

Jungwon Park

Jungwon Park received his B.S. degree from the Department of Chemistry, POSTECH, South Korea, in 2003, and his Ph.D. degree from the Department of Chemistry, University of California, Berkeley, in 2012. After a post-doc at the School of Engineering and Applied Sciences, Harvard University, he started a faculty position at the School of Chemical and Biological Engineering, Seoul National University, in 2016, and he currently serves as an associate professor jointly affiliated with the Center for Nanoparticle Research, Institute for Basic Science (IBS). His research area includes the in situ *study of nanomaterials, liquid-phase TEM, phase transitions, interface chemistry, and low-dimensional materials.*

Results and discussion

The realistic 3D atomic structures of individual single-crystalline Pt nanoparticles were obtained by the Brownian one-particle reconstruction method,[18,19] revealing that the structures of the PVP-passivated Pt nanoparticles are nonuniformly deviated from the bulk face-centered-cubic structure of Pt (Fig. 1a and b). The surface structures of the synthesized Pt nanoparticles are complicated due to the irregular shapes of islands, resulting in a diverse distribution of the generalized coordination number ($\overline{\mathrm{CN}}$) (Fig. 1a). The $\overline{\mathrm{CN}}$ is an extension of the coordination number (CN) considering the CNs of the first nearest neighbor atoms surrounding a surface atom of interest. The definition of the CN is shown in the Methods section in the ESI.† The $\overline{\mathrm{CN}}$ of an atom i enclosed by the first nearest neighbor atoms j is defined by

$$\overline{\mathrm{CN}_i} = \sum_{k=1}^{i} \frac{\mathrm{CN}(k)}{\mathrm{CN}_{\max}}, \quad (1)$$

where $\mathrm{CN}_{\max}$ and $\mathrm{CN}(k)$ denote the maximum CN of the first nearest neighbor atoms and the CN of each first nearest neighbor atom, respectively. According to eqn (1), the $\overline{\mathrm{CN}}$ indicates a distinct local geometry of a surface atom. Thus, a diverse distribution of the $\overline{\mathrm{CN}}$ means that the synthesized nanoparticles consist of various surface atoms with different local geometries. This implies that ligands could strongly interact with surface atoms and that the way they passivate the surface is complicated. In addition, the various surface structures cover much broader training space for the ANN than model nanoparticles, which improves the accuracy of prediction of ligand adsorption behavior on Pt nanoparticles (Fig. S1†).

From the 3D atomic structures, surface atoms were defined as ones that have a CN $\leq$ 9 and meet the following surface vector criteria (Fig. 1a and S2†): each Pt cluster was clipped from the center Pt with a cutoff radius (10 Å in Fig. S2†).[16] The surface vector was defined as a normalized vector starting from the center of mass of neighboring Pt to center Pt. If all angles between the center Pt to neighboring Pt vector and the surface vector were larger than 30 degrees, the center Pt met the criteria and is extracted as a surface atom. The Pt cluster clipped with a cutoff of 10 Å well represents the adsorption behavior of PVP on the Pt surface, as shown in the benchmark calculation (Fig. 1b and S3†). It was modeled that a PVP monomer consists of a pyrrolidone ring, and an ethane group could bind to the top of Pt binding sites. Density functional theory (DFT) was corrected with the DFT-D3 method to analyze the complex PVP adsorption behavior involving short-range direct bonding energy (E_{bind}) and long-range van der Waals interaction energy (E_{vdW}) (Fig. 1c). Ligand binding energy (E_{ads}) is calculated from the summation of E_{bind} and E_{vdW} (Fig. 1c and eqn (2)).

$$E_{\mathrm{ads}} = E_{\mathrm{bind}} + E_{\mathrm{vdW}} \quad (2)$$

The degree of freedom from the azimuthal binding angle was considered. The training data for the ANN was constructed

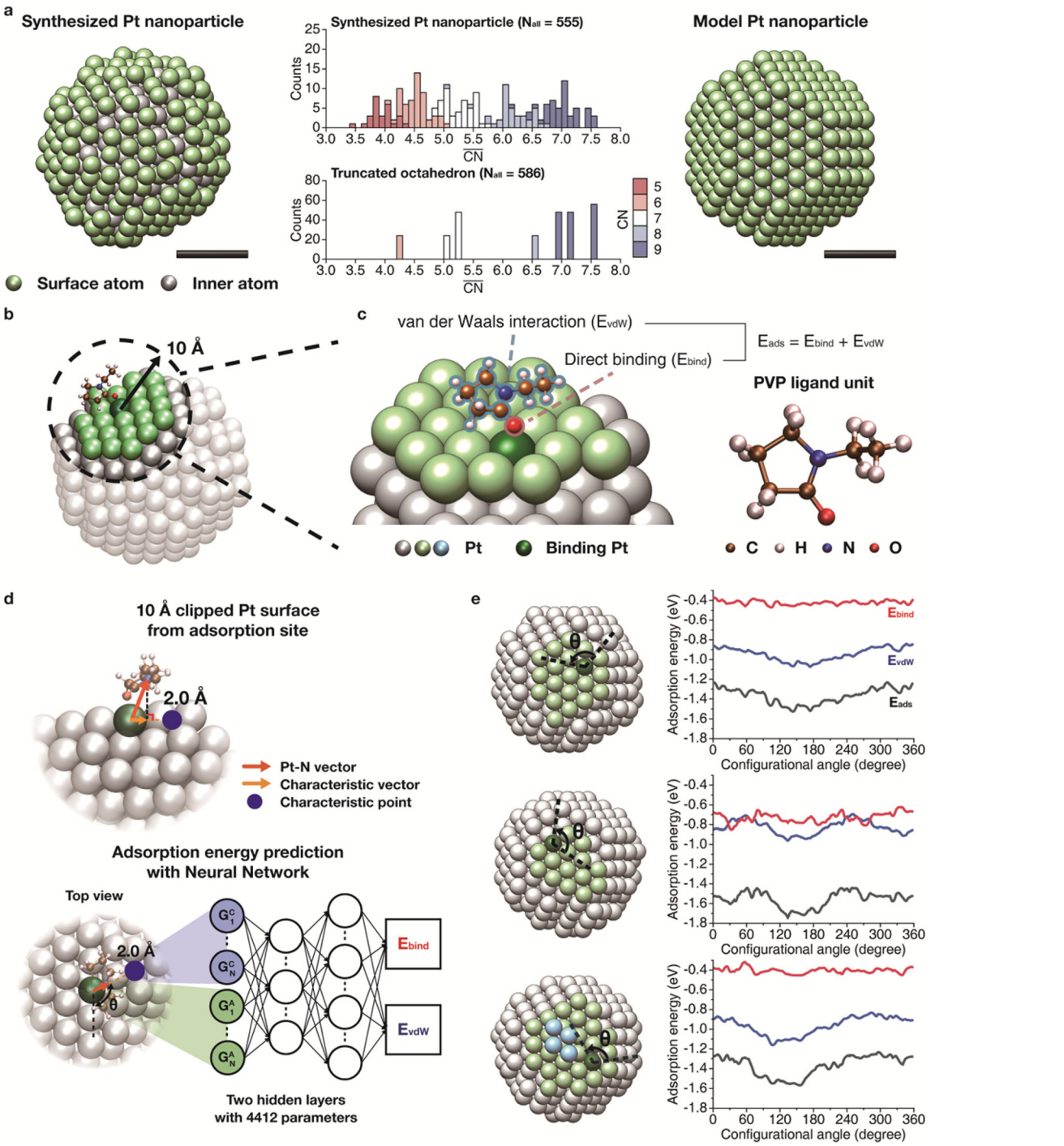

Fig. 1 Scheme for machine-learning-accelerated *ab initio* calculation. (a) Representative 3D structures of the synthesized and model nanoparticles shown on the left and right sides, respectively. The histograms for the $\overline{CN}$ of surface atoms on both nanoparticles are presented in the middle panel. The histograms of the synthesized and model nanoparticles are shown at the top and bottom, respectively. (b) The surface structure of the PVP ligand protected Pt nanoparticle is clipped around 10 Å. (c) DFT-D3 calculated ligand binding energy (E_{ads}) is used for the training set. (d) Local geometric information is extracted as a set of symmetry functions from the adsorption site (the green atom, G_i^A) and the characteristic point (the blue point, G_i^C) where the orientation of the PVP monomer, θ, is reflected. Each of the two hidden layers of the fully connected neural network consists of 30 nodes and 60 nodes, respectively. (e) The angular adsorption energy profiles of the PVP ligand on the different types of surface structures of particle 1 can be predicted by the ANN. The red, blue and black lines indicate E_{bind}, E_{vdW} and E_{ads}, respectively.

by extensive DFT calculations for PVP adsorption. 1386 configurations representing 231 surface atoms of Pt nanoparticle 1 in Fig. 1 including azimuthally-rotated PVP orientations with 60-degree intervals for each site were initially screened. Among them, 452 configurations which PVP could not access were removed from the data. In addition, 32 configurations were

also excluded, which showed direct bonding by the nitrogen atom of PVP. This binding mode is often observed for larger nanoparticles (~8.4 nm), while it is negligible for smaller nanoparticles (~6.4 nm and smaller) where the carbonyl binding mode is dominant.[10] Note that our Pt nanoparticles have sizes ranging from 2 nm to 3 nm and have been reconstructed from an environment where the PVP ligands dynamically interact with Pt surfaces, whose fluctuations potentially induce the dominance of the carbonyl bonding mode. Thus, the oxygen-binding mode of 902 configurations was eventually utilized for the training process.

The symmetry function was used for the input feature to predict the adsorption energy of PVP on the Pt adsorption center as shown in Fig. 1d.[20] To handle the degree of freedom of azimuthally θ-rotated PVP, a characteristic point that represents the local geometry information from the PVP orientation was assigned. The characteristic vector was defined as the projection of the Pt adsorption center to the nitrogen atom (the Pt–N vector in Fig. 1d) on the surface of a Pt cluster. The characteristic point was defined as the point 2.0 Å away from the adsorption center in the direction of the characteristic vector. The distance between the adsorption center and the characteristic point was determined by a 5-fold cross-validation (Table S1†). We calculated 40 symmetry functions from the adsorption center and characteristic point (12 for the radial part and 28 for the angular part) and concatenated them to make an input feature with 80 dimensions (see the Methods section in the ESI†). The produced input feature was used by a two-layered fully connected neural network with 4412 hidden parameters to predict the E_{vdW} and E_{bind}, respectively. By using the ANN, the angular adsorption energy profiles of PVP on various Pt nanoparticle surface structures can be deduced, as shown in Fig. 1e. Since ligands can dynamically interact with the metal nanoparticle surface by adsorption and desorption processes,[9] the θ-averaged adsorption energy is used to represent the binding affinity of PVP for Pt adsorption centers.

The dataset with a total of 902 configurations was split into 722 configurations for the training set, 90 for the validation set, and 90 for the test set with the same coordination group ratio as in the original dataset. We kept track of the validation data for adjusting the learning rate with the learning rate scheduler to prevent overfitting. The evolution of training and validation errors during the training epoch is shown in Fig. S4.† Training was stopped early at epoch 716, with a root mean square error (RMSE) of 0.2169 eV for the training set and an RMSE of 0.2250 eV for the validation set. Fig. 2a and b show the prediction results for the test set with RMSE values of 0.0519 eV and 0.0708 eV for E_{vdW} and E_{bind}, error levels comparable to those for the adsorption of simple adsorbates (CO and HOCO) in a previous study.[16]

The surface atoms of each synthesized Pt nanoparticle 1 to 6 are displayed with a color gradient according to the θ-averaged E_{bind}, E_{vdW} and E_{ads} assigned for each surface atom, respectively (Fig. 2c and d, and Fig. S5†). For the E_{bind} and E_{ads} maps, the adsorption centers on the terrace show low binding energy, while the others on the edges and kinks show high binding energy. This result is consistent with previous results obtained from an ideal Pt surface.[10] However, the E_{vdW} maps show higher binding energies on the edges and kinks than for the atoms on the terrace. In addition, the distributions of averaged E_{bind} for each nanoparticle are different from those of averaged E_{vdW} (Fig. S6 and S7†). As shown in the histograms of the averaged E_{bind} and E_{vdW} for each nanoparticle, the energy distributions of E_{bind} are close to a bimodal shape, while those of E_{vdW} are close to a unimodal distribution. We calculated the bimodality index (BI) for the energy distributions, representing the level of bimodal distribution, which shows that the distributions of E_{bind} have a higher BI than those of E_{vdW} for all Pt nanoparticles (Fig. S8 and see the Methods section in the ESI†). These findings indicate that the two types of ligand binding modes are differently affected by the Pt surface structures.

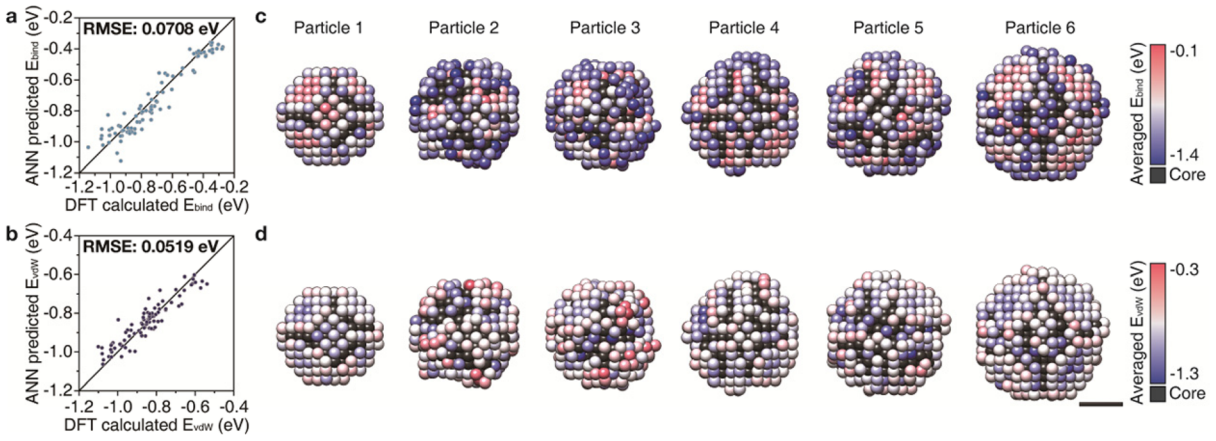

Fig. 2 (a and b) Artificial neural network prediction results of the test set for (a) E_{bind} with a root mean square error of 0.0708 eV and (b) E_{vdW} with a root mean square error of 0.0519 eV. (c and d) The 3D atomic structures of the six synthesized Pt nanoparticles colored based on (c) θ-averaged E_{bind} and (d) θ-averaged E_{vdW} of the PVP ligand. Each Pt nanoparticle has a diameter of 2.25, 2.41, 2.42, 2.52, 2.66, and 2.92 nm, respectively. Scale bar, 1 nm.

CN and $(\overline{CN})$ are descriptors associated with the chemical activities of surface atoms. It is known that the CN and $\overline{CN}$ show a strong linear relationship with the adsorption energies of simple adsorbates such as O, O_2, OOH, and OCH_3 on high-symmetry metal nanoparticles.[21–25] However, unlike the simple adsorbates, the correlation between the ANN-predicted averaged PVP binding energy (E_{ads}) and the $\overline{CN}$ of an adsorption center shows a weak positive relationship of linear correlation with a Pearson correlation coefficient (r) of ~0.656 (Fig. 3a).

Following the different trends of energy distributions in Fig. 2c and d, averaged E_{bind} and E_{vdW} show different correlations with the $\overline{CN}$ (Fig. 3b and c). The correlation between the E_{bind} and $\overline{CN}$ is highly linear with a positive trend, because

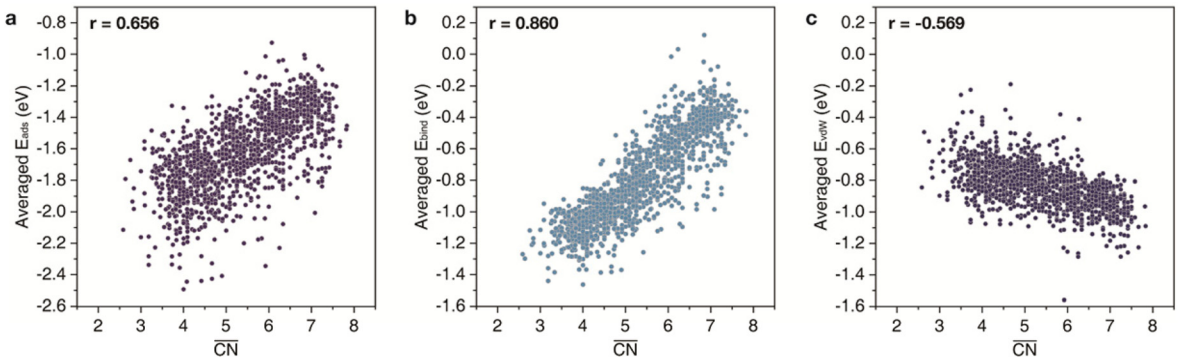

Fig. 3 (a) Correlation between the $\overline{CN}$ of the adsorption centers and the θ-averaged adsorption energies predicted by the ANN. (b) Correlation between the $\overline{CN}$ of the adsorption centers and the energy contribution of direct bonding. (c) Correlation between the $\overline{CN}$ of the adsorption centers and the energy contribution of the van der Waals interaction.

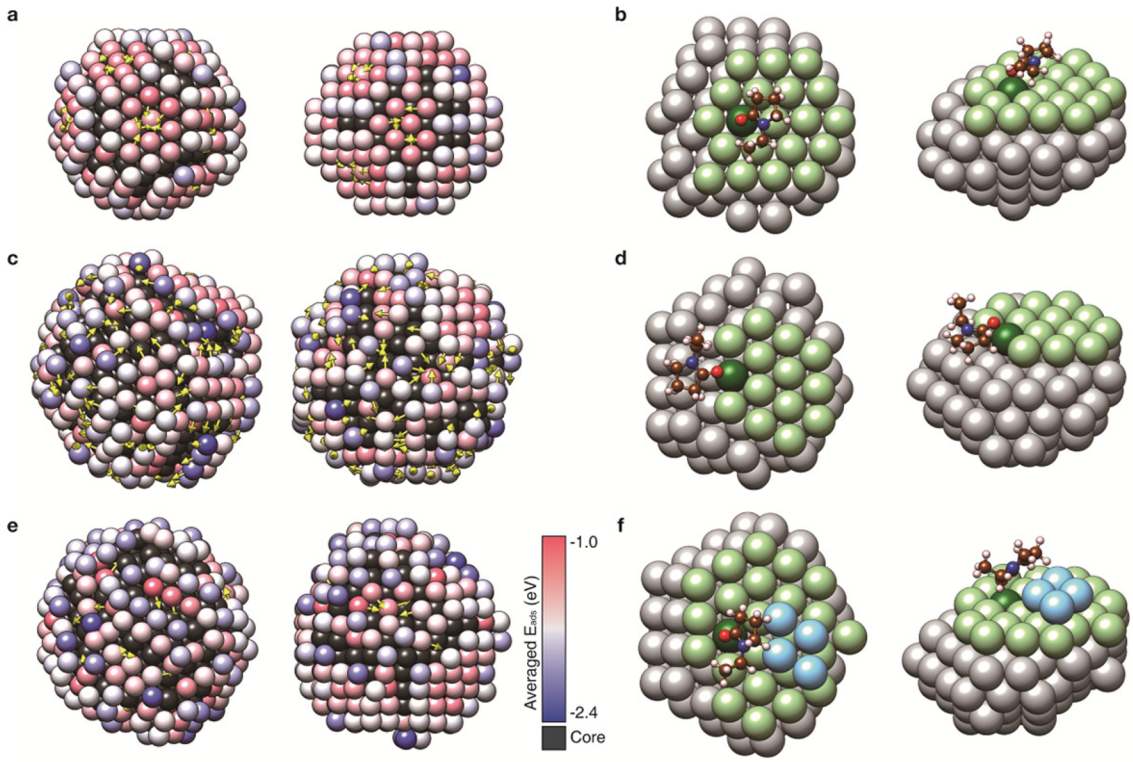

Fig. 4 (a, c and e) 3D maps of averaged adsorption energy, with yellow arrows indicating the characteristic vectors of the adsorbed PVP ligands with the lowest E_{vdW}. The PVP ligands are adsorbed onto (a) particle 1, (c) particle 5, and (e) particle 4. The arrows come from the (a) terraces, (c) edges, and corners, and (e) from under the islands. (b, d and f) Examples for the optimal configurations of the PVP ligands adsorbed on the different surface structures of particle 1 (the (left) top-view and (right) side-view are shown). The PVP ligands are adsorbed on (b) a terrace, (d) an edge, and (f) under the islands.

direct bonding of PVP by the O atom of the carbonyl group is predominantly governed by the degree of dangling bonds of the adsorbed Pt surface atom.[26] On the other hand, E_{vdW} shows a weak negative relationship with the $\overline{CN}$. Since long-range interactions with the surrounding Pt surfaces are also involved in the pyrrolidone ring and ethane group, E_{vdW} does not exhibit a noticeable relationship with the $\overline{CN}$, which is relevant to the coordination environment of an adsorption center. These different correlations with the $\overline{CN}$ indicate that the weak positive relationship between the E_{ads} and $\overline{CN}$ is attributed to the van der Waals interactions of the large-sized ligands, and the long-range interaction significantly contributes to the adsorption between the large-sized ligands and the complex surfaces of the nanoparticles. Note that the Pearson correlation coefficient of the E_{bind} to $\overline{CN}$ is still lower than the one from the ideal structures reported in previous studies because of the low-symmetry structure of the synthesized Pt nanoparticles.[22]

The negative relationship of the E_{vdW} with the $\overline{CN}$ indicates that the pyrrolidone ring and ethane group strongly interact with the surrounding Pt surfaces when PVP binds to the Pt adsorption center with a high $\overline{CN}$, such as the terrace and the step; however, they weakly interact when the adsorption centers have low $\overline{CN}$ values, such as the edge and the corner. Since the long-range interaction is predominantly governed by the degree of contact between the PVP ligand and the Pt surface, the energy profiles along the different angular configurations of PVP show that the energy deviation of E_{vdW} is larger than that of E_{bind} (Fig. S9†). Thus, the configuration of adsorbed PVP on the Pt surfaces with the lowest value of E_{vdW}, meaning the most stable van der Waals interaction, is required to investigate the relationship of the E_{vdW} with $\overline{CN}$. For the adsorption directions with the lowest E_{vdW}, the characteristic vectors (the projection of the Pt–N vector on the Pt surface, Fig. 1c) are shown as yellow arrows on the 3D atomic maps of Pt nanoparticles (Fig. 4a, c, and e).

The adsorption directions on the Pt nanoparticle surfaces with the lowest E_{vdW} have the following tendency. First, when the PVP ligands directly bind to the terrace atoms of islands, they are more likely to direct toward the nearby terrace atoms

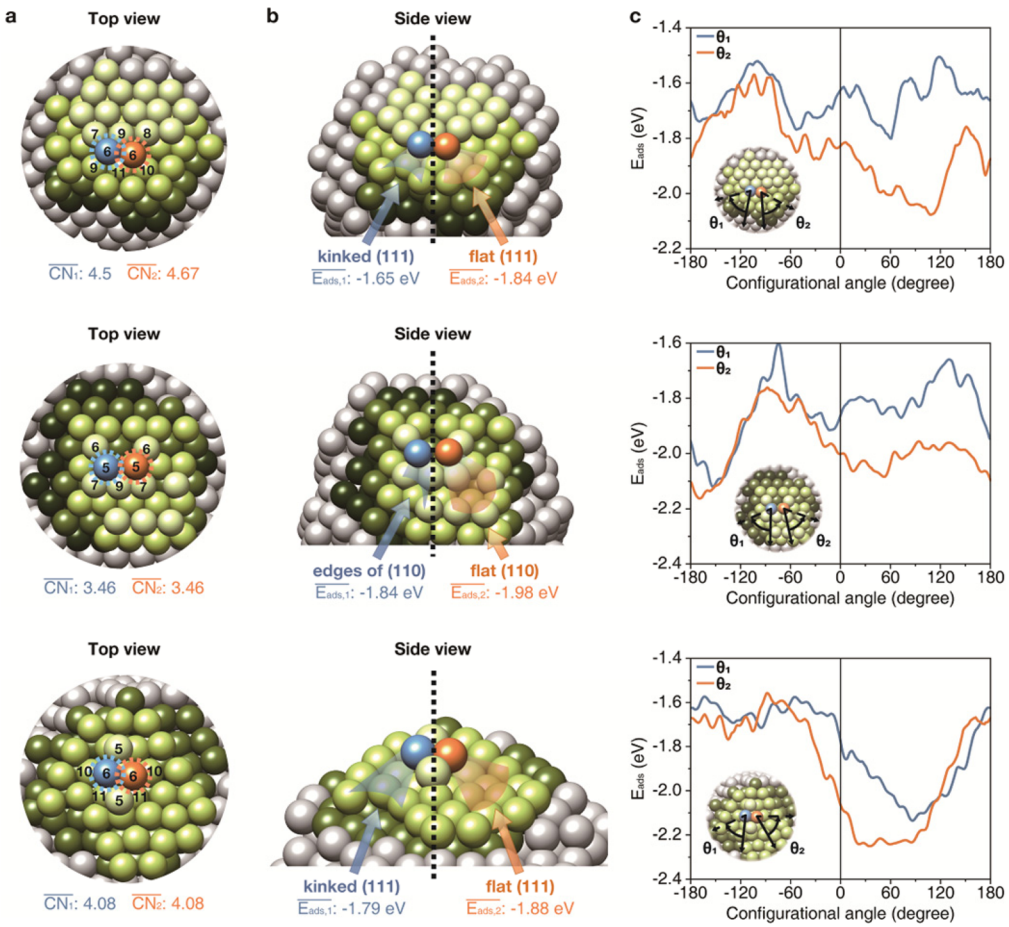

Fig. 5 (a) Top view of the exemplary adsorption sites with a similar $\overline{CN}$ but different adsorption energies. The constituent atoms included in the 10 Å cluster for the ANN prediction are colored according to depth. The coordination numbers of the adsorption centers and their nearest neighbors are indicated. (b) Side view of the exemplary adsorption centers. The auxiliary lines serve as a guide for comparing the local geometry of each adsorption site. The θ-averaged adsorption energies of each adsorption center are presented. (c) Angular adsorption energy profiles on each adsorption center.

(Fig. 4a, b, and Fig. S10†). Second, the PVP ligands binding on the edge and corner atoms prefer to locate toward the steps nearby (Fig. 4c, d, and Fig. S11†). Third, the PVP ligands binding on the adsorption centers under the islands tend to adsorb toward the steps nearby (Fig. 4e, f, and Fig. S12†). These results indicate that a way to maximize the degree of contact of PVP ligands depends on the type of adsorption center, which leads to a weak negative relationship between the E_{vdW} and $\overline{CN}$. In addition, when comparing the adsorption direction of each PVP ligand with the lowest E_{bind} and E_{vdW} and the adsorption direction with the lowest E_{ads}, the configurational similarity with the lowest E_{vdW} is higher than that of the lowest E_{bind} (Fig. S13†). This indicates that the PVP ligands prefer to adsorb where the long-range vdW interaction with the surrounding surface structure is maximized. In other words, the surrounding surface geometry of an adsorption center is important in determining the most stable configuration of the binding PVP ligands on the low-symmetry surface structure of Pt nanoparticles.

The PVP adsorption behavior on several adsorption centers with the same CN and similar $\overline{CN}$ was carefully examined to represent the influence of the surrounding surface geometry on the adsorption energy. Two adsorption centers for each particle with the same CN are colored in blue and orange (Fig. 5a and b). Although each pair shows similar $\overline{CN}$ values, the averaged adsorption energy of each adsorption center differs by more than 0.1 eV (Fig. 5b). This is because the local surface geometry surrounding the adsorption center is different, as shown in the top view and side view (Fig. 5a and b). In detail, the local surface geometry around the higher binding energy site shows a flat surface, while the lower binding energy site is surrounded by kinks and edges. This implies that the flat pyrrolidone ring of PVP favors neighboring flat surfaces with high van der Waals interaction. The binding energy for the sites even with the same $\overline{CN}$ also shows difference in its angular profile (Fig. 5c). The large difference in the adsorption energies at a specific configurational angle is also shown in the results of the DFT calculation (Table S2†). The results show that the adsorption energy of PVP ligands is significantly affected by each surrounding geometry.

The observation we found is also consistent with previous reports where PVP ligand adsorption on ideal surfaces such as (100) and (111) facets was studied.[10–14] For example, Saidi *et al.* reported that the vdW interaction is stronger on Ag(111) than on Ag(100) because of a higher local density of surface atoms.[11,14] In our work, realistic nanoparticle surfaces composed of various low-symmetry surfaces are considered. Interestingly, following the negative correlation of the E_{vdW} with the $\overline{CN}$ in Fig. 3, surface atoms in Pt(111) $\left(\overline{CN} = 7.5\right)$ show higher E_{vdW} interaction than the ones in Pt(100) $\left(\overline{CN} = 6.67\right)$, consistent with the results from the ideal surfaces.[10–14] Likewise, our machine-learning-accelerated *ab initio* calculation can address various kinds of low-symmetry adsorption centers with additional rotation degrees of freedom of PVP ligands. Note that the symmetry functions we exploited in the ANN can also be applied to the machine learning potential which is powerful to optimize the configuration and calculate the energies of various systems. We adopted an ANN to consider the dynamic interaction of PVP on low-symmetry surfaces, which can analyze adsorption behavior at different angular configurations regardless of the large dependence on the initial configuration of coordinate optimization in DFT and machine learning potential. With more careful consideration of the training, prediction process, and broader dataset, we expect that sophisticated machine learning potential will facilitate larger scale simulations including the effects of solvents and polymer chains.

Conclusions

In summary, we calculated the adsorption energy of PVP ligands on the synthesized Pt nanoparticles and analyzed their adsorption behavior through machine-learning-accelerated *ab initio* calculation. The use of experimentally resolved atomic structures of nanoparticles provides sufficiently diverse sampling data for learning the adsorption tendency on realistic nanoparticle surfaces and enables accurate prediction of surface chemistry. We revealed that the negative relationship of the E_{vdW} with the $\overline{CN}$ attenuates the strong positive relationship of E_{bind}, which leads to a weak positive relationship of the E_{ads} of the PVP ligand. In addition, we showed that the PVP ligands prefer to adsorb where the long-range vdW interaction with the surrounding surface structure is maximized. Our results emphasize the significant contribution of vdW interactions and the importance of the local geometry of surface atoms to the adsorption behavior of large-sized ligands on low-symmetry surfaces. The introduced method utilizing machine-learning-accelerated *ab initio* calculation and experimentally analyzed surface atomic structures suggests a new low-cost and high-precision computational approach for studying surface chemistry and catalytic activity of nanoparticles.

Author contributions

D. K. and S. K. contributed equally to this work. D. K., S. K., and J. P. planned the research. D. K., S. K., J. H., and J. P. acquired the 3D atomic structures. D. K., D. K., and H. B. calculated PVP adsorption energy with DFT. D. K. trained the ANN to predict PVP adsorption energy. D. K., S. K., J. H., S. K., and J. P. analyzed and interpreted the results. D. K., S. K., J. H., D. K., H. B., S. K., S. S., H. L., and J. P. wrote the manuscript. S. S., H. L., and J. P. supervised the research. All authors contributed to the discussion of results.

Data availability

The Cartesian coordinates of the constituent atoms in the Pt nanocrystals shown in this paper are posted on a public website (**https://parklab.snu.ac.kr/resources**).

Conflicts of interest

There are no conflicts of interest to declare.

Acknowledgements

J. P. acknowledges the Institute for Basic Science (IBSR006-D1). D. K., S. K., J. H., S. K., and J. P. acknowledge the National Research Foundation of Korea (NRF) grant funded by the Korean government (MSIT) (NRF-2020R1A2C2101871). D. K., S. K., J. H., D. K., S. K., and J. P. acknowledge the National Research Foundation of Korea (NRF) grant funded by the Korean government (MSIT) (NRF-2019M3E6A1064877). D. K., S. K., D. K., S. K., and J. P. acknowledge the support provided by the Samsung Science and Technology Foundation under project no. SSTFBA1802-08 for sample preparation and method development. J. H. and J. P. acknowledge the National Research Foundation of Korea (NRF) grant funded by the Korean government (MSIT) (NRF-2017R1A5A1015365). Theoretical computation was supported by the National Supercomputing Center with supercomputing resources including technical support (KSC-2020-CRE-0310).

References

1 A. Dong, X. Ye, J. Chen, Y. Kang, T. Gordon, J. M. Kikkawa and C. B. Murray, *J. Am. Chem. Soc.*, 2011, **133**, 998–1006.
2 H. J. Yun, T. Paik, M. E. Edley, J. B. Baxter and C. B. Murray, *ACS Appl. Mater. Interfaces*, 2014, **6**, 3721–3728.
3 S. N. Sheikholeslami, H. Alaeian, A. L. Koh and J. A. Dionne, *Nano Lett.*, 2013, **13**, 4137–4141.
4 Y. Xia, Y. Xiong, B. Lim and S. E. Skrabalak, *Angew. Chem., Int. Ed.*, 2009, **48**, 60–103.
5 X. Xia, J. Zeng, L. K. Oetjen, Q. Li and Y. Xia, *J. Am. Chem. Soc.*, 2012, **134**, 1793–1801.
6 N. Geva, J. J. Shepherd, L. Nienhaus, M. G. Bawendi and T. Van Voorhis, *J. Phys. Chem. C*, 2018, **122**, 26267–26274.
7 S. M. Ansar, R. Haputhanthri, B. Edmonds, D. Liu, L. Yu, A. Sygula and D. Zhang, *J. Phys. Chem. C*, 2011, **115**, 653–660.
8 Z. Hens and J. C. Martins, *Chem. Mater.*, 2013, **25**, 1211–1221.
9 J. De Roo, M. Ibáñez, P. Geiregat, G. Nedelcu, W. Walravens, J. Maes, J. C. Martins, I. Van Driessche, M. V. Kovalenko and Z. Hens, *ACS Nano*, 2016, **10**, 2071–2081.
10 J.-Y. Ye, G. A. Attard, A. Brew, Z.-Y. Zhou, S.-G. Sun, D. J. Morgan and D. J. Willock, *J. Phys. Chem. C*, 2016, **120**, 7532–7542.
11 W. A. Saidi, H. Feng and K. A. Fichthorn, *J. Phys. Chem. C*, 2013, **117**, 1163–1171.
12 S. Back, M. S. Yeom and Y. Jung, *ACS Catal.*, 2015, **5**, 5089–5096.
13 S. Back, H. Kim and Y. Jung, *ACS Catal.*, 2015, **5**, 965–971.
14 W. Al-Saidi, H. Feng and K. A. Fichthorn, *Nano Lett.*, 2012, **12**, 997–1001.
15 R. Gasper, H. Shi and A. Ramasubramaniam, *J. Phys. Chem. C*, 2017, **121**, 5612–5619.
16 Y. Chen, Y. Huang, T. Cheng and W. A. Goddard III, *J. Am. Chem. Soc.*, 2019, **141**, 11651–11657.
17 G. H. Gu, J. Lim, C. Wan, T. Cheng, H. Pu, S. Kim, J. Noh, C. Choi, J. Kim and W. A. Goddard III, *J. Am. Chem. Soc.*, 2021, **143**, 5355–5363.
18 B. H. Kim, J. Heo, S. Kim, C. F. Reboul, H. Chun, D. Kang, H. Bae, H. Hyun, J. Lim and H. Lee, *Science*, 2020, **368**, 60–67.
19 S. Kim, J. Kwag, C. Machello, S. Kang, J. Heo, C. F. Reboul, D. Kang, S. Kang, S. Shim and S.-J. Park, *Nano Lett.*, 2021, **21**, 1175–1183.
20 J. Behler and M. Parrinello, *Phys. Rev. Lett.*, 2007, **98**, 146401.
21 T. Jiang, D. Mowbray, S. Dobrin, H. Falsig, B. Hvolbæk, T. Bligaard and J. K. Nørskov, *J. Phys. Chem. C*, 2009, **113**, 10548–10553.
22 F. Calle-Vallejo, J. Tymoczko, V. Colic, Q. H. Vu, M. D. Pohl, K. Morgenstern, D. Loffreda, P. Sautet, W. Schuhmann and A. S. Bandarenka, *Science*, 2015, **350**, 185–189.
23 F. Calle-Vallejo, M. D. Pohl and A. S. Bandarenka, *ACS Catal.*, 2017, **7**, 4355–4359.
24 B. Han, C. Miranda and G. Ceder, *Phys. Rev. B: Condens. Matter Mater. Phys.*, 2008, **77**, 075410.
25 F. Calle-Vallejo, D. Loffreda, M. Koper and P. Sautet, *Nat. Chem.*, 2015, **7**, 403–410.
26 L. Qiu, F. Liu, L. Zhao, W. Yang and J. Yao, *Langmuir*, 2006, **22**, 4480–4482.